Li, Yingying; Ma, Xueli; Lv, Wei; Chen, Hong; Yu, Linhao; Ma, Zewei; Wang, Sen; Li, Yongdan

Efficient Selective Oxidation of 5-Hydroxymethylfurfural with Oxygen over a ZnCrAl Mixed Oxide Catalyst Derived from Hydrotalcite-like Precursor

Published in:
Industrial and Engineering Chemistry Research

DOI:
10.1021/acs.iecr.2c00886

Published: 10/08/2022

Document Version
Publisher's PDF, also known as Version of record

I&EC research
Industrial & Engineering Chemistry Research

pubs.acs.org/IECR

Article

Efficient Selective Oxidation of 5-Hydroxymethylfurfural with Oxygen over a ZnCrAl Mixed Oxide Catalyst Derived from Hydrotalcite-like Precursor

Yingying Li, Xueli Ma, Wei Lv, Hong Chen,* Linhao Yu, Zewei Ma, Sen Wang, and Yongdan Li*

Cite This: *Ind. Eng. Chem. Res.* 2022, 61, 11597−11603

Read Online

ACCESS | Metrics & More | Article Recommendations

ABSTRACT: Cr-doped ZnAl mixed oxide catalysts ($Zn_{0.75}$CrAl-*x*-c) were obtained via calcining the $Zn_{0.75}$CrAl-*x* hydrotalcite precursors and were applied in the selective oxidation of 5-hydroxymethylfurfural (5-HMF) to 2,5-furandicarboxylic acid (FDCA). Cr doping significantly enhanced the catalytic activity. A 95.1% 5-HMF conversion with an 88.1% FDCA selectivity was achieved over the $Zn_{0.75}$CrAl-6-c catalyst at 130 °C under 0.6 MPa oxygen for 4 h. The good performance was associated with the high specific surface area and high oxygen vacancy concentration. Moreover, the $Zn_{0.75}$CrAl-6-c catalyst was used for five cycles without a significant activity loss indicating excellent stability.

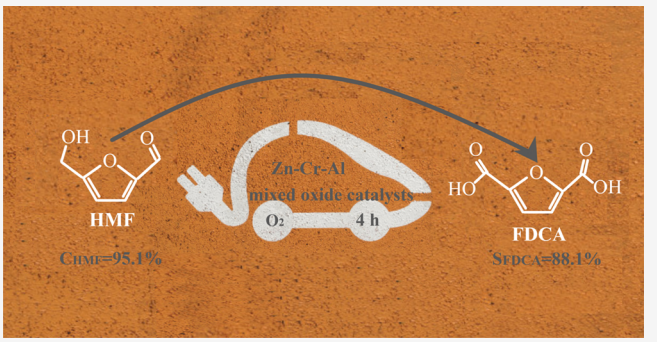

INTRODUCTION

Oxygen-containing chemical production from fossil resources is often energy-intensive, and thus, exploitation and utilization of oxygen-containing feedstocks such as lignocellulosic biomass have aroused attention in the production of value-added chemicals as well as fuels in the beginning of the 21st century. The production of oxygen-containing chemicals such as furfural, 5-hydroxymethylfurfural (5-HMF), and 2,5-furandicarboxylic acid (FDCA) from biomass resources will not only minimize the energy consumption and cost of the feedstocks but also reduce the environmental concerns in society.[1−4]

FDCA is one of the top 12 high-value chemicals derived from biomass and has been used as an important renewable substitute for terephthalic acid, which has been produced from petroleum, to produce plastics, and as a raw material for the production of medical anesthetics.[5−7]

Biomass-derived 5-HMF can be converted to FDCA through an oxidation reaction, for which the formation of byproducts, e.g., 2,5-diformylfuran, 5-hydroxymethyl-2-furancarboxylic acid, and 5-formyl-2-furancarboxylic acid, has been a challenge. At present, the main ways to realize the efficient catalytic conversion of HMF to FDCA include thermal, electro-, and photocatalysis. Among them, electro- and photocatalysis have become promising catalytic routes for clean and green preparation of FDCA from HMF due to the advantages of mild reaction conditions, environmental friendliness, and high selectivity. Liu et al.[8] reported ternary NiCoMn-layered double hydroxide (NiCoMn-LDH) nanosheets as efficient electrochemical catalysts with abundant oxygen vacancies, and a 91.7% FDCA yield could be obtained under mild conditions for 2.5 h. Xu et al.[9] immobilized cobalt−sulfur porphyrin thioporphyrin (CoPz) in g-C_3N_4 solution to prepare a CoPz/g-C_3N_4 photocatalyst and achieved a 95% FDCA yield after 14 h under optimal reaction conditions. The current catalytic routes based on electro- and photocatalysis show excellent performance. However, with the reaction device components not yet standardized and usually requiring high production cost, they are still in the stage of laboratory model studies.

For the preparation of FDCA, the thermal catalytic oxidation of HMF has been extensively studied on various catalysts. Homogeneous catalysts, such as Mn(III)−salen, $Co(OAc)_2$/$Mn(OAc)_2$/HBr, etc.,[10,11] usually have highly catalytic activity and high selectivity. However, homogeneous catalytic systems retain some intractable drawbacks, such as difficulty in reuse and environmental pollution.[11] Numerous studies have confirmed that noble metal catalysts, such as Au, Pt, and Pd,[12−15] generally exhibit better activity and FDCA selectivity under mild reaction conditions but also have disadvantages of excess strong base additives and high price.[16,17] Therefore, from the perspective of environmental protection and economy, it is necessary to develop efficient, stable, and low-cost nonprecious metal catalysts for the oxidative conversion of 5-HMF to HMF.

Received: March 16, 2022
Revised: July 19, 2022
Accepted: July 20, 2022
Published: July 29, 2022

https://doi.org/10.1021/acs.iecr.2c00886
Ind. Eng. Chem. Res. 2022, 61, 11597−11603

Hayashi et al.[18] obtained a 74% FDCA yield over the MnO_2 catalyst for 24 h under 1 MPa O_2 and at 100 °C. With cobalt and cerium bimetallic catalysts, an 83.6% FDCA yield was achieved at 130 °C in DMF for 4 h.[19] All these studies showed that non-noble metal catalysts are particularly economical and efficient in the catalytic conversion of HMF to FDCA, but there are still some drawbacks, such as nonenvironment-friendly catalyst preparation, complicated steps, and harsh reaction conditions.

In recent years, mixed metal oxide catalysts, generally with a uniform metal ion dispersion, large surface area, basic surface property, and high stability, prepared with roasting hydrotalcite-structured precursors have been used as efficient catalysts in transesterification and oxidation reactions.[20−22] However, only a limited number of works focused on the selective oxidation of 5-HMF. Neşu et al.[23] used a manganese−copper mixed oxide catalyst prepared from layered double hydroxide in HMF selective oxidation and obtained a 90% HMF conversion and an 87% DFF selectivity under 8.0 MPa oxygen pressure in 24 h. Raut and Bhanage[24] reported a cobalt−aluminum hydrotalcite-derived mixed metal oxide catalyst and applied the catalyst in the one-pot and two-step DFF synthesis from fructose. A 77.0% DFF yield was obtained at 120 °C for 8 h under 3.0 MPa O_2.

Here, we report a zinc−chromium−aluminum mixed oxide, derived from a hydrotalcite-structured precursor, as a promising catalyst in the selective oxidation of HMF to FDCA.

EXPERIMENTAL SECTION

Materials. 5-HMF (98.0%), FDCA (97.0%), and DFF (98.0%) were purchased from J&K Chemical Co., Ltd. (Beijing, China). Sodium hydroxide (NaOH, 96.0%) was obtained from Kermel Chemical Reagent Co., Ltd. (Tianjin, China). Aluminum(III) nitrate hexahydrate ($Al(NO_3)_3·6H_2O$, 99.0%) was bought from Macklin Biochemical Technology Co., Ltd. (Shanghai, China). Chromium(III) nitrate nonahydrate ($Cr(NO_3)_3·9H_2O$, 99.0%) was from Yien Chemical Scientific Co., Ltd. (Shanghai, China). Zinc(II) nitrate hexahydrate ($Zn(NO_3)_3·6H_2O$, 99.0%) was from Titan Scientific Co., Ltd. (Shanghai, China). Anhydrous sodium carbonate (Na_2CO_3, 98.0%) was from Fengchuan Chemical Reagent Technology Co., Ltd. (Tianjin, China). *N*,*N*-Dimethylformamide (DMF, 99.0%), dimethyl sulfoxide (DMSO, 99.0%), methanol (MeOH, 99.0%), and acetonitrile (MeCN, 99.0%) were purchased from Aladdin Chemical Reagent Co., Ltd. (Shanghai, China). All the chemicals were used without further treatment. Deionized water, with a resistivity of >18.0 MΩ/cm, was prepared from a Barnstead ultrapure water purifier.

Catalyst Preparation. All the catalyst samples were synthesized with a coprecipitation method. In a typical procedure, $Zn(NO_3)_3·6H_2O$ (5.59 g), $Cr(NO_3)_3·9H_2O$ (0.36−0.69 g), and $Al(NO_3)_3·9H_2O$ (1.76−2.00 g) were dissolved in deionized water under stirring with ultrasonication to obtain a mixed salt solution. Then, the solution was slowly dripped into 1 M Na_2CO_3 solution. Meanwhile, the pH value was monitored with a pH meter in real time. Then, the mixed solution was kept under vigorous stirring for 2 h at 70 °C, and then, the pH was adjusted to 7.0 by gently adding 1 M NaOH solution. The slurry was aged for about 4 h at 70 °C and then filtrated with distilled water until the pH was 7.0 and dried overnight at 70 °C. The obtained zinc−chromium−aluminum hydrotalcite materials were denoted as $Zn_{0.75}$CrAl-*x*. *x* represents the molar ratio of Al and Cr.

The $Zn_{0.75}$CrAl-*x* sample was calcined at 460 °C for 6 h to obtain the hydrotalcite-derived mixed oxide catalyst ($Zn_{0.75}$CrAl-*x*-c). ZnO, Al_2O_3, and Cr_2O_3 samples were obtained by the precipitation of $Zn(NO_3)_3·6H_2O$, $Al(NO_3)_3·9H_2O$, and $Cr(NO_3)_3·9H_2O$, respectively.

Catalyst Characterization. X-ray diffraction (XRD) patterns of the samples were acquired with a D8-Focus diffractometer made by Bruker AXS Co., Ltd., using a Cu Kα radiation source (λ = 1.5418 Å) in the 2θ range of 10−70° at a scanning rate of 10°/min. The analysis was taken at 40 kV and 200 mA. The specific surface area of the catalyst was obtained under the conditions of 78.3 K nitrogen physical adsorption (QUA211007, Quantachrome, USA). Before the measurement, the sample was degassed for 4 h in vacuum at 150 °C. The surface morphology of the catalysts was observed with a Hitachi Regulus 8100 scanning electron microscope (SEM). The valence state changes and oxygen species of Co and Cr in the catalyst were measured with an ESCALAB-250Xi X-ray photoelectron spectroscopy (XPS) instrument from Thermo Fisher Scientific, and the results were calibrated referring to the C 1s peak at 284.8 eV. The chemical composition of the samples was reconfirmed by inductively coupled plasma-optical emission spectroscopy (ICP-OES) with an iCAP7000 series spectrometer.

Catalytic Activity Measurement. Catalytic reactions were carried out in a 150 mL Teflon-lined stainless-steel autoclave equipped with an oil bath with a magnetic stirrer. In a typical experiment, about 50 mg of catalyst, 50 mg of Na_2CO_3, and 1 mmol of HMF were added into the autoclave reactor containing 25 mL of DMF. The reactor was sealed and afterward purged with O_2 three times. The reactor was then pressurized up to 0.6 MPa O_2 and heated up to the required temperature with a stirring rate of 500 rpm. After the reactor was cooled down to room temperature, the reaction mixture was collected and separated using a 0.2 μm polytetrafluoroethylene filter. The products were analyzed with a high-performance liquid chromatograph (HPLC) equipped with a UV detector and a reversed-phase C18 column. A mixture of acetonitrile and water with a volume ratio of 3:7 was used as the mobile phase at 25 °C with a flow rate of 1 mL/min. The corresponding peaks of the products were identified with standard samples, and the products were quantified with the external standard curve method. The conversion of HMF, selectivity, and yield of products were calculated with eqs 1, 2, and 3, respectively.

$$\text{conversion}\ (\%) = \frac{n_{\text{HMF},0} - n_{\text{HMF},t}}{n_{\text{HMF},0}} \quad (1)$$

$$\text{selectivity}\ (\%) = \frac{n_{\text{product}}}{n_{\text{HMF},0} - n_{\text{HMF},t}} \quad (2)$$

$$\text{yield}\ (\%) = \frac{n_{\text{product}}}{n_{\text{HMF},0}} \quad (3)$$

$n_{\text{HMF},0}$ is the initial molar amount of 5-HMF, $n_{\text{HMF},t}$ is the molar amount of 5-HMF after the reaction, and n_{product} is the molar amount of the product after the reaction.

RESULTS

Characterization of the Catalyst. The XRD patterns of the hydrotalcite-like precursors and mixed solids calcined at 460 °C are displayed in Figure 1. For $Zn_{0.75}$Al, $Zn_{0.75}$CrAl-6, and $Zn_{0.75}$CrAl-9 samples, all the peaks in the patterns at 2θ = 11, 23, 34, 39, 46, 60, and 61° are characteristic of the hydrotalcite structure,[25,26] corresponding to the (003), (006), (012), (015),

https://doi.org/10.1021/acs.iecr.2c00886
Ind. Eng. Chem. Res. 2022, 61, 11597−11603

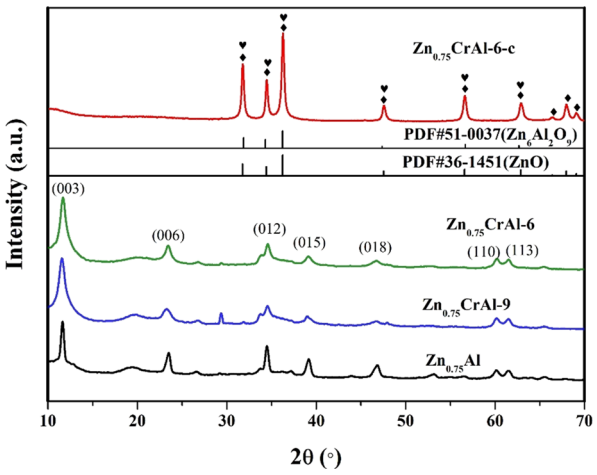

Figure 1. X-ray diffraction patterns of catalysts and precursors.

(018), (110), and (113) crystal planes, respectively. Two obvious diffraction peaks appear near $2\theta = 60°$, which indicate that the interlayer cations and the layer anions are evenly arranged.[27,28] It is noted that the peak width of the characteristic peaks increases due to the doping of chromium. Considering the Scherrer formula, this suggests that the two Cr-doped precursors have relatively smaller crystallite sizes, which contribute to the high dispersion of the corresponding calcined samples. The XRD pattern of the derived composite oxide $Zn_{0.75}$CrAl-6-c, from the calcination of $Zn_{0.75}$CrAl-6, is also plotted in Figure 1, showing only the diffraction peaks of ZnO (PDF no. 36-1451) and $Zn_6Al_2O_9$ (PDF no. 51-0037) phases. The diffraction peaks of Cr-containing phases are not observed, suggesting the formation of solid solution of Cr^{3+} with both ZnO and $Zn_6Al_2O_9$ phases.

The specific surface area of the catalysts was measured with the BET method (Table 1). The $Zn_{0.75}$CrAl-6 sample gives a higher specific surface area than that of the $Zn_{0.75}$CrAl-9 sample, no matter whether in the dried or calcined state. All the surface areas of the $Zn_{0.75}$CrAl-x samples increase after calcination. Among the samples, $Zn_{0.75}$CrAl-6-c has the largest specific surface area of 75 m^2 g^{-1}. The chemical composition in the samples was reconfirmed according to the ICP-OES results. The data in Table 1 show that the compositions of all samples are basically consistent with the prescribed values, with reasonable variation within the experimental error range of the ICP technique.

Table 1. Surface Area and Chemical Composition of the Synthesized Catalyst Samples

		nominal content		ICP results	
catalyst	surface area (m^2/g)	Zn/Al ratio	Al/Cr ratio	Zn/Al ratio	Al/Cr ratio
$Zn_{0.75}$CrAl-6	51	3.5	6	3.53	5.70
$Zn_{0.75}$CrAl-9	35	3.3	9	3.27	8.85
$Zn_{0.75}$CrAl-6-c	75	3.5	6	3.51	5.60
$Zn_{0.75}$CrAl-9-c	49	3.3	9	3.23	8.79

The morphologies of $Zn_{0.75}$CrAl-x and $Zn_{0.75}$CrAl-x-c are examined with the SEM technique. Figure 2a,c shows that both samples $Zn_{0.75}$CrAl-6 and $Zn_{0.75}$CrAl-9 before calcination are composed of platelet-like agglomerated crystals, which represent the characteristics of layered clay materials.[29,30] Compared to

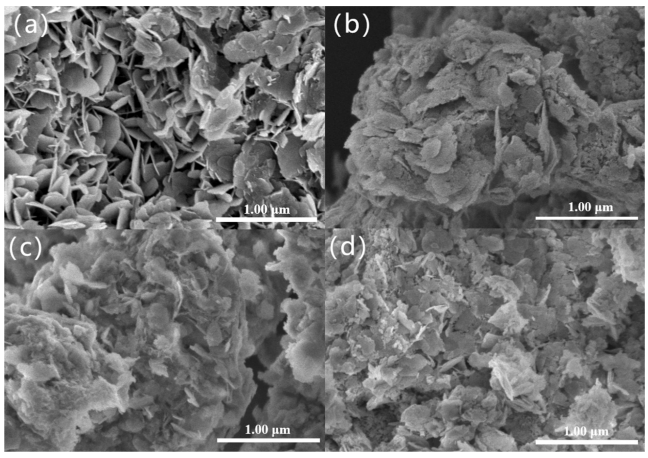

Figure 2. SEM micrographs of Cr-doped catalysts and precursors. (a) $Zn_{0.75}$CrAl-6, (b) $Zn_{0.75}$CrAl-6-c, (c) $Zn_{0.75}$CrAl-9, and (d) $Zn_{0.75}$ CrAl-9-c.

$Zn_{0.75}$CrAl-9, the structure of $Zn_{0.75}$CrAl-6 becomes fluffier, which makes it have a larger external surface area.[31] After calcination at 460 °C, the hydrotalcite structure collapses and both the samples become flocculent (Figure 2b,d)

The O 1s and Cr 2p spectra of the fresh $Zn_{0.75}$CrAl-6-c and used $Zn_{0.75}$CrAl-6-c catalyst samples are given in Figure 3. In Figure 3a, the O 1s spectra display 3 major oxygen species with the corresponding peaks at 529.8, 531.4, and 532.8 eV, which are assigned to lattice oxygen ($O_{Lattice}$), oxygen vacancies or surface-adsorbed oxygen ions and/or OH groups ($O_{Vacancies}$), and adsorbed molecular water ($O_{Adsorbed}$), respectively.[32,33] The oxygen vacancy content on the fresh $Zn_{0.75}$CrAl-6-c (36.2%) is higher than that on the used $Zn_{0.75}$CrAl-6-c (17.3%). As shown in Figure 3b, both the fresh and used $Zn_{0.75}$CrAl-6-c Cr 2p spectra have two main peaks, corresponding to Cr $2p_{3/2}$ and Cr $2p_{1/2}$.[34] These two main peaks are deconvoluted into four separate components. The peaks at 576.0 and 586.6 eV are ascribed to Cr^{3+} species on the catalysts surface, while the peaks at around 578.5 and 584.8 eV are responsible for the existence of Cr^{6+}. The contents of Cr^{6+} species are calculated to be 49.9 and 47.4% for the fresh and used $Zn_{0.75}$CrAl-6-c samples, respectively.

The Oxidation Reaction. The catalytic activity measurement results of all the prepared catalyst samples are summarized in Table 2. When the $Zn_{0.75}$Al-c catalyst was employed, only a 24.0% conversion of HMF and a 75.8% selectivity of FDCA were obtained. The great improvements of both 5-HMF conversion (58.8%) and FDCA selectivity (78.4%) were achieved over the $Zn_{0.75}$CrAl-9 catalyst. The higher Cr doping amount also shows a positive effect on the HMF conversion and FDCA selectivity, where a 61.2% conversion of 5-HMF and a 79.2% selectivity of FDCA were observed with the $Zn_{0.75}$CrAl-6 catalyst. The $Zn_{0.75}$CrAl-6-c catalyst showed the best activity in the oxidation of 5-HMF to FDCA with a 95.1% 5-HMF conversion and an 88.1% FDCA selectivity. As a comparison, ZnO and Al_2O_3 as catalysts were also measured but exhibited only moderate activities, with 36.9 and 35.8% HMF conversions and 70.7 and 78.7% FDCA selectivities, respectively. When Cr_2O_3 was used alone as a catalyst, the HMF conversion was 89.9% and the FDCA selectivity was 79.2%.

The Effect of Reaction Conditions. The amount of catalyst shows a significant effect on the 5-HMF conversion and FDCA selectivity in Figure 4a. Without a catalyst, the 5-HMF

https://doi.org/10.1021/acs.iecr.2c00886
Ind. Eng. Chem. Res. 2022, 61, 11597−11603

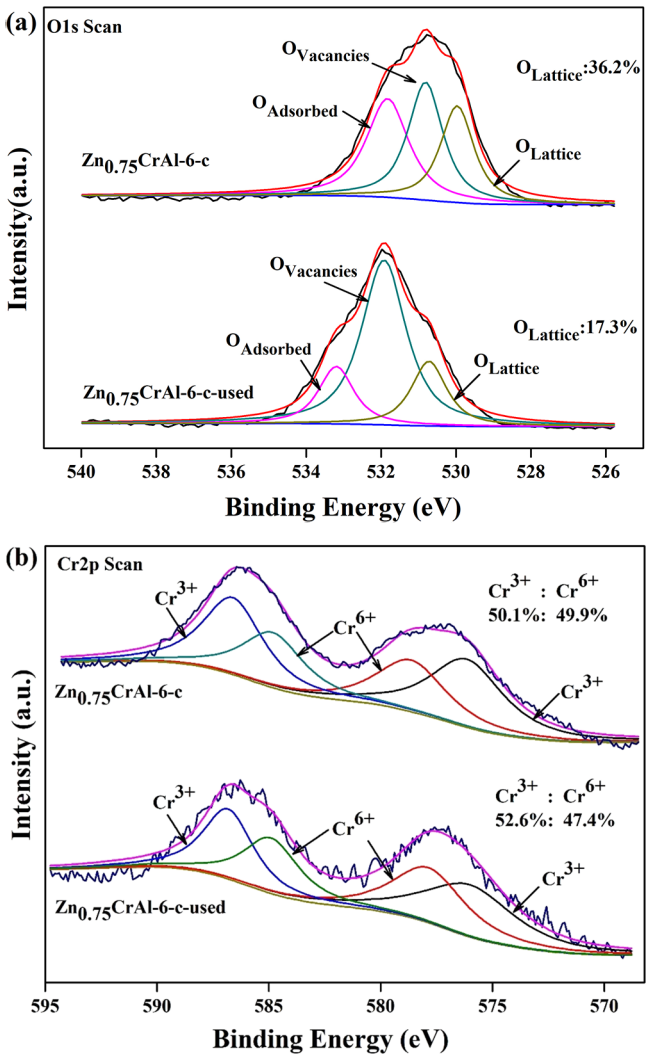

Figure 3. XPS spectra of (a) O 1s and (b) Cr 2p scans of the fresh $Zn_{0.75}CrAl$-6-c and used $Zn_{0.75}CrAl$-6-c samples.

Table 2. The Oxidation of 5-HMF to FDCA over the Catalyst Samples

			selectivity (%)[b]		
entry[a]	catalyst	conversion (%)	FDCA	DFF	others
1	$Zn_{0.75}CrAl$-6	61.2	79.2	2.1	18.7
2	$Zn_{0.75}CrAl$-9	58.8	78.4	2.7	18.9
3	$Zn_{0.75}CrAl$-6-c	95.1	88.1	0.9	11.0
4	$Zn_{0.75}CrAl$-9-c	83.8	85.5	1.2	13.3
5	$Zn_{0.75}Al$-c	24.0	75.8		24.2
6	ZnO	36.9	70.7	1.5	27.8
7	Al_2O_3	35.8	78.7		21.3
8	Cr_2O_3	89.9	79.2	1.4	19.4

[a]Reaction conditions: 1 mmol of 5-HMF, 50 mg of catalyst, 50 mg of Na_2CO_3, 25 mL of DMF, 130 °C, 4 h, 0.6 MPa O_2, and 500 rpm stirring. [b]The results are obtained by HPLC with the external standard technique and a GC−MS instrument.

conversion and FDCA selectivity were 30.3 and 35.5%, respectively. In the range of 0−100 mg, both the 5-HMF conversion and FDCA selectivity increased with the increase of the catalyst amount. Nevertheless, the increases of both the conversion and selectivity are moderate in the range of 25 to 100

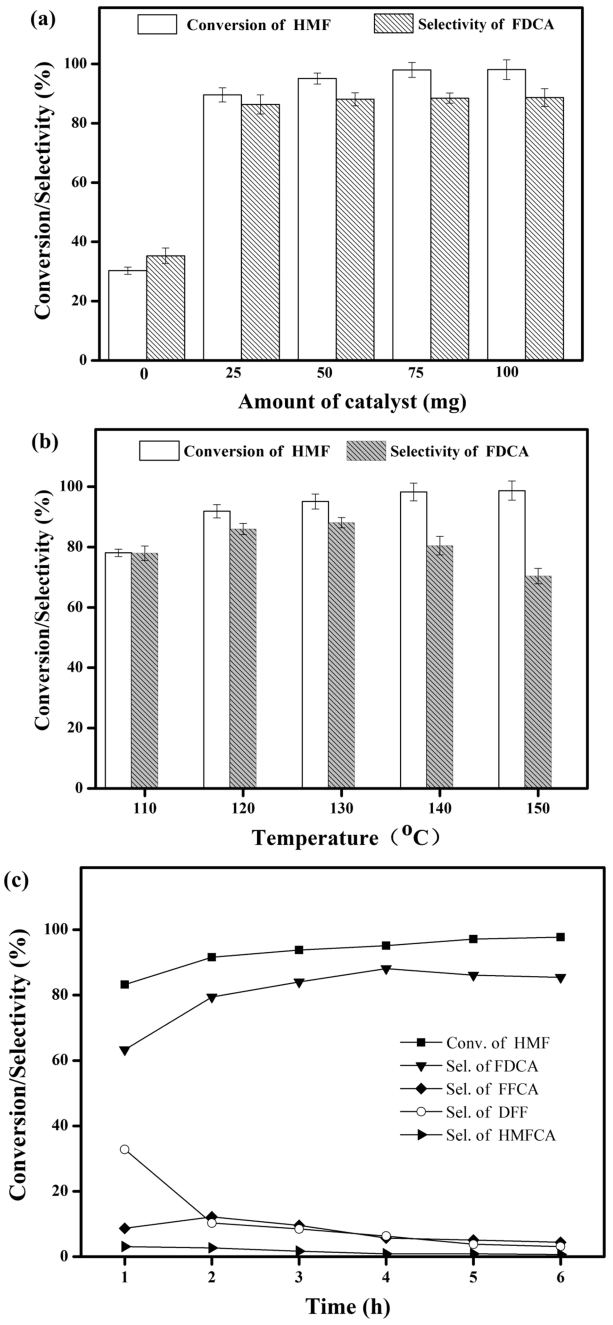

Figure 4. Catalytic performance of $Zn_{0.75}CrAl$-6-c at different (a) catalyst amounts, (b) reaction temperatures, and (c) reaction times. (a) Reaction conditions: W(HMF) = 0.126 g; V(DMF) = 25 mL; T = 130 °C; $P(O_2)$ = 0.6 MPa; t = 4 h; $W(Na_2CO_3)$ = 0.05 g; 500 rpm stirring. (b) Reaction conditions: W(HMF) = 0.126 g; V(DMF) = 25 mL; W(catalyst) = 0.05 g; $P(O_2)$ = 0.6 MPa; t = 4 h; $W(Na_2CO_3)$ = 0.05 g; 500 rpm stirring. (c) Reaction conditions: W(HMF) = 0.126 g; V(DMF) = 25 mL; W(catalyst) = 0.05 g; T = 130 °C; $P(O_2)$ = 0.6 MPa; $W(Na_2CO_3)$ = 0.05 g; 500 rpm stirring.

mg. The conversion of 5-HMF kept a monotonic increase from 78.1 to 98.7% when the reaction temperature increased from 110 to 150 °C, but the FDCA selectivity exhibited the maximum value of 88.1% at 130 °C (Figure 4b). Figure 4c depicts the effect of reaction time on the oxidation reaction. The 5-HMF conversion kept a monotonic increase to 95.1% in the initial 4 h and then reached 97.7% at 6 h. The selectivity of FDCA gave a maximum value of 88.1% at 4 h. After that, the FDCA selectivity

https://doi.org/10.1021/acs.iecr.2c00886
Ind. Eng. Chem. Res. 2022, 61, 11597−11603

Scheme 1. Reaction Pathways for Aerobic Oxidation of HMF to FDCA

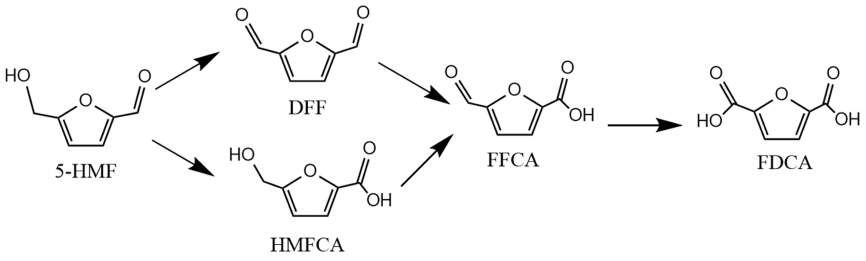

turned stable as the time continued. The selectivity of the intermediate HMFCA increased to 3.1% in the initial 1 h and then gradually decreased along with the reaction time. The DFF and FFCA selectivity reached the highest value at 2 h and started to decrease afterward. These results indicated that the oxidation of HMF to FDCA over the $Zn_{0.75}$CrAl-6-c catalyst is a multistep tandem pathway reaction, as shown in Scheme 1.

Recyclability. The recycle experiment with the $Zn_{0.75}$CrAl-6-c catalyst sample was carried out in five consecutive runs under the identical optimal conditions: 1 mmol of 5-HMF, 50 mg of $Zn_{0.75}$CrAl-6-c catalyst, 50 mg of Na_2CO_3, 25 mL of DMF, 0.6 MPa O_2, and 500 rpm stirring. After each run, the solid catalyst was separated and washed with deionized water three times. The solid sample was dried in air for 12 h before characterization. As shown in Figure 5, the conversion and FDCA selectivity were

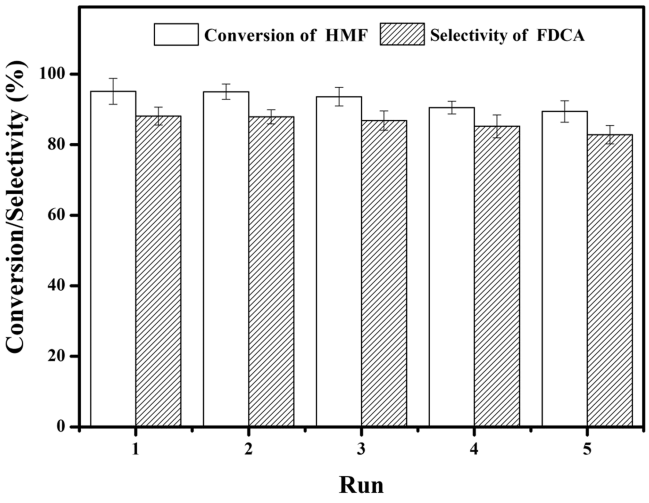

Figure 5. Recyclability tests for the HMF oxidation over the $Zn_{0.75}$CrAl-6-c catalyst. Reaction conditions: 1 mmol of 5-HMF, 50 mg of $Zn_{0.75}$CrAl-6-c, 50 mg of Na_2CO_3, 25 mL of DMF, 0.6 MPa O_2, and 500 rpm stirring.

95.1 and 88.1%, respectively, for the first run, and in the fifth run, the two values were 89.4 and 82.8%, respectively. It can be concluded that the $Zn_{0.75}$CrAl-6-c catalyst sample exhibits good stability in the HMF oxidation reaction.

DISCUSSION

The Precursor and Catalysts. The XRD characteristic peaks of the $Zn_{0.75}$Al-*x* coprecipitate precursors are similar to that of the $Zn_{0.75}$Al sample, and the XRD patterns of all the precursors are consistent with that of the standard XRD pattern of the hydrotalcite-like double-layer hydroxide compound. These results mean that the preparation of a uniform mixed oxide catalyst is successful. The SEM micrographs of the Cr-containing hydrotalcite-like compounds have a typical layered structure. After calcination, the double-layer hydroxide structure collapsed due to the loss of water and carbonate ions. The resulting mixed oxide does not show any peaks of Cr oxides in the XRD pattern, but the pattern only indicates the existence of the solid solution containing Cr^{3+} and taking the structures of $Zn_6Al_2O_9$ and ZnO. The $Zn_{0.75}$CrAl-6-c sample exhibits a loose morphology in the SEM micrograph and has a large value of the BET surface area, which improves the contact between the catalyst and the reactant, thus enhancing the catalytic activity. According to the XPS results, three types of oxygen species exist on the $Zn_{0.75}$CrAl-6-c surface. $O_{Lattice}$ acts as a nucleophilic reagent and is responsible for the selective oxidation reaction.[35] $O_{Vacancies}$ help to improve the high catalytic activity and promote the rate of oxygen replenishment on the catalyst surface.[36,37] The signal of lattice oxygen decreased and the oxygen vacancies increased on the used $Zn_{0.75}$CrAl-*x*-c, implying that the oxidation of 5-HMF to FDCA proceeded via the Mars−van Krevelen mechanism and the lattice oxygen was involved in the oxidation reaction.

The Role of the Catalyst and Catalytic Sites. The HMF oxidation reaction happens without a catalyst, but both the conversion and yield are low. With the presence of $Zn_{0.75}$Al as a catalyst, the HMF conversion reached 24.0% and the FDCA selectivity achieved 75.8%. Meanwhile, a large amount of other products, 24.2%, was measured in the product stream, indicating a low selectivity. $Zn_{0.75}$Al has a low activity in redox reactions due to the high electron exchange energy barriers of the composing metal ions. Therefore, $Zn_{0.75}$Al mixed oxides often show an intrinsic property as a solid base. The conversion of 5-HMF on this mixed oxide may be due to the coexistence of weak redox Zn−O−Al pairs and the weak basic sites (OH− groups). However, such basic site-catalyzed oxidation reactions are not selective enough. Similar results were obtained when ZnO, Al_2O_3, and Cr_2O_3 were used as the catalysts, see entries 6−8 in Table 2. With the doping of Cr to the Zn−Al hydrotalcite-structured compound, both the conversion of HMF and the yield of FDCA are enhanced. After calcination of the double hydroxide precursor, the mixed oxide catalysts containing Cr are further improved toward HMF selective oxidation to FDCA. The sample $Zn_{0.75}$CrAl-6-c exhibits an HMF conversion of 95.1% and an FDCA selectivity of 88.1%. This excellent activity and selectivity can be explained by the XPS results. For the $Zn_{0.75}$CrAl-6-c catalyst, after the reaction, the contents of Cr^{6+} and lattice oxygen were both decreased, and those of Cr^{3+} and oxygen vacancies were both increased, demonstrating that Cr^{6+} and lattice oxygen were converted and reduced to Cr^{3+} and oxygen vacancies, respectively. Thus, the reaction could be following the Mars−van Krevelen mechanism.

Effect of the Reaction Conditions. With the increase of the catalyst amount from 0 to 50 mg, both 5-HMF conversion and FDCA selectivity increased notably, demonstrating that the

https://doi.org/10.1021/acs.iecr.2c00886
Ind. Eng. Chem. Res. 2022, 61, 11597−11603

availability of catalytic active sites is crucial to the acceleration of the reaction rate. When 100 mg of catalyst was used, the number of active sites reached the maximum value and the further increase of the catalyst amount did not improve the conversion and selectivity further.

The increase of the reaction temperature increases the HMF conversion, but above 130 °C, a further increase of the temperature leads to the decrease of the FDCA selectivity, indicating that the positive effect of molecular activation is limited in an appropriate range.[38] The instability of HMF at high temperatures and the side reactions in an oxidation atmosphere lead to the formation of byproducts such as ring-opened molecules and other deep oxidation species, which has been discussed in the literature.[36,39,40] In this work, 5-HMF conversion reached 95.1% at 130 °C for around 4 h.

In the period of 2−4 h, the FDCA yield increased with the time increased. After 4 h, both the yields of FDCA and FFCA, the major byproduct, become quite stable until 6 h with low yield values of FFCA, indicating that FFCA is an intermediate to FDCA and during the prolonged time period of >4 h, the reaction approaches the thermodynamic equilibrium with low concentration values of FFCA in the system.

CONCLUSIONS

In this work, Cr-doped ZnAl mixed oxide catalysts were prepared through a novel method involving the calcination of hydrotalcite-like structured precursors for the selective catalytic oxidation of 5-HMF to FDCA. A calcined catalyst named as $Zn_{0.75}$CrAl-6-c achieved a 95.1% HMF conversion and an 88.1% FDCA selectivity at 130 °C under 0.6 MPa O_2 pressure for 4 h. In addition, the catalyst can be reused more than five times without an obvious loss of activity (around 5%). The good catalytic performance of the $Zn_{0.75}$CrAl-6-c catalyst was attributed to its high specific surface area and high oxygen vacancy concentration, which promote the lattice oxygen replenishment of the catalyst via the Mars−van Krevelen mechanism. We believe that $Zn_{0.75}$CrAl-6-c is a promising catalyst and has great potential application in the production of value-added chemicals from biomass-derived compounds.

AUTHOR INFORMATION

Corresponding Authors

Hong Chen − *School of Environmental Science and Engineering, Tianjin University, Tianjin 300072, China;* orcid.org/0000-0002-0325-2786; Email: chenhong_0405@tju.edu.cn

Yongdan Li − *Collaborative Innovation Centre of Chemical Science and Engineering (Tianjin), Tianjin Key Laboratory of Applied Catalysis Science and Technology, State Key Laboratory of Chemical Engineering, School of Chemical Engineering and Technology, Tianjin University, Tianjin 300072, China; Department of Chemical and Metallurgical Engineering, School of Chemical Engineering, Aalto University, Espoo 02150, Finland;* orcid.org/0000-0002-0430-9879; Email: yongdan.li@aalto.fi

Authors

Yingying Li − *School of Environmental Science and Engineering, Tianjin University, Tianjin 300072, China*

Xueli Ma − *School of Environmental Science and Engineering, Tianjin University, Tianjin 300072, China*

Wei Lv − *School of Environmental Science and Engineering, Tianjin University, Tianjin 300072, China*

Linhao Yu − *Collaborative Innovation Centre of Chemical Science and Engineering (Tianjin), Tianjin Key Laboratory of Applied Catalysis Science and Technology, State Key Laboratory of Chemical Engineering, School of Chemical Engineering and Technology, Tianjin University, Tianjin 300072, China*

Zewei Ma − *Collaborative Innovation Centre of Chemical Science and Engineering (Tianjin), Tianjin Key Laboratory of Applied Catalysis Science and Technology, State Key Laboratory of Chemical Engineering, School of Chemical Engineering and Technology, Tianjin University, Tianjin 300072, China*

Sen Wang − *School of Environmental Science and Engineering, Tianjin University, Tianjin 300072, China*

Complete contact information is available at: https://pubs.acs.org/10.1021/acs.iecr.2c00886

Author Contributions

Y.L. performed the methodology and investigation and wrote the original draft; Z.M. and Y.L. reviewed and edited the manuscript; W.L. and S.W. performed formal and software analysis; H.C. performed supervision and conceptualization and reviewed and edited the manuscript; L.Y. performed conceptualization and reviewed and edited the manuscript; X.M. performed visualization.

Notes

The authors declare no competing financial interest.

ACKNOWLEDGMENTS

The work was supported by the Natural Science Foundation of China (21808163).

REFERENCES

(1) Kasipandi, S.; Ali, M.; Li, Y.; Bae, J. W. Phosphorus-Modified Mesoporous Inorganic Materials for Production of Hydrocarbon Fuels and Value-Added Chemicals. *ChemCatChem* **2020**, *12*, 4224−4241.

(2) Sheldon, R. A. The Road to Biorenewables: Carbohydrates to Commodity Chemicals. *ACS Sustainable Chem. Eng.* **2018**, *6*, 4464−4480.

(3) Melero, J. A.; Iglesias, J.; Garcia, A. Biomass as renewable feedstock in standard refinery units. Feasibility, opportunities and challenges. *Energy Environ. Sci.* **2012**, *5*, 7393−7420.

(4) Cardiel, A. C.; Taitt, B. J.; Choi, K.-S. Stabilities, Regeneration Pathways, and Electrocatalytic Properties of Nitroxyl Radicals for the Electrochemical Oxidation of 5-Hydroxymethylfurfural. *ACS Sustainable Chem. Eng.* **2019**, *7*, 11138−11149.

(5) Cousin, T.; Galy, J.; Rousseau, A.; Dupuy, J. Synthesis and properties of polyamides from 2,5-furandicarboxylic acid. *J. Appl. Polym. Sci.* **2018**, *135*, 45901−45912.

(6) Papageorgiou, G. Z.; Papageorgiou, D. G.; Terzopoulou, Z.; Bikiaris, D. N. Production of bio-based 2,5-furan dicarboxylate polyesters: Recent progress and critical aspects in their synthesis and thermal properties. *Eur. Polym. J.* **2016**, *83*, 202−229.

(7) Lewkowski, J. Synthesis, chemistry and applications of 5-hydroxymethylfurfural and its derivatives. *ARKIVOC* **2001**, *34*, 17−54.

(8) Liu, B.; Xu, S.; Zhang, M.; Li, X.; Decarolis, D.; Liu, Y.; Wang, Y.; Gibson, E. K.; Catlow, C. R. A.; Yan, K. Electrochemical upgrading of biomass-derived 5-hydroxymethylfurfural and furfural over oxygen vacancy-rich NiCoMn-layered double hydroxides nanosheets. *Green Chem.* **2021**, *23*, 4034−4043.

(9) Xu, S.; Zhou, P.; Zhang, Z.; Yang, C.; Zhang, B.; Deng, K.; Bottle, S.; Zhu, H. Selective Oxidation of 5-Hydroxymethylfurfural to 2,5-Furandicarboxylic Acid Using O_2 and a Photocatalyst of Co-thioporphyrazine Bonded to g-C_3N_4. *J. Am. Chem. Soc.* **2017**, *139*, 14775−14782.

(10) Amarasekara, A. S.; Green, D.; McMillan, E. Efficient oxidation of 5-hydroxymethylfurfural to 2,5-diformylfuran using Mn(III)−salen catalysts. *Catal. Commun.* **2008**, *9*, 286−288.
(11) Partenheimer, W.; Grushin, V. V. Synthesis of 2,5-Diformylfuran and Furan-2,5-Dicarboxylic Acid by Catalytic Air-Oxidation of 5-Hydroxymethylfurfural. Unexpectedly Selective Aerobic Oxidation of Benzyl Alcohol to Benzaldehyde with Metal/Bromide Catalysts. *Adv. Synth. Catal.* **2001**, *343*, 102−111.
(12) Sang, B.; Li, J.; Tian, X.; Yuan, F.; Zhu, Y. Selective aerobic oxidation of the 5-hydroxymethylfurfural to 2,5-furandicarboxylic acid over gold nanoparticles supported on graphitized carbon: Study on reaction pathways. *Mol. Catal.* **2019**, *470*, 67−74.
(13) Zhou, C.; Deng, W.; Wan, X.; Zhang, Q.; Yang, Y.; Wang, Y. Functionalized Carbon Nanotubes for Biomass Conversion: The Base-Free Aerobic Oxidation of 5-Hydroxymethylfurfural to 2,5-Furandicarboxylic Acid over Platinum Supported on a Carbon Nanotube Catalyst. *ChemCatChem* **2015**, *7*, 2853−2863.
(14) Lei, D.; Yu, K.; Li, M.-R.; Wang, Y.; Wang, Q.; Liu, T.; Liu, P.; Lou, L.-L.; Wang, G.; Liu, S. Facet Effect of Single-Crystalline Pd Nanocrystals for Aerobic Oxidation of 5-Hydroxymethyl-2-furfural. *ACS Catal.* **2017**, *7*, 421−432.
(15) Yi, G.; Teong, S. P.; Zhang, Y. Base-free conversion of 5-hydroxymethylfurfural to 2,5-furandicarboxylic acid over a Ru/C catalyst. *Green Chem.* **2016**, *18*, 979−983.
(16) Liu, W.; Dang, L.; Xu, Z.; Yu, H.; Jin, S.; Huber, G. W. Electrochemical Oxidation of 5-Hydroxymethylfurfural with NiFe Layered Double Hydroxide (LDH) Nanosheet Catalysts. *ACS Catal.* **2018**, *8*, 5533−5541.
(17) Bonincontro, D.; Lolli, A.; Storione, A.; Gasparotto, A.; Berti, B.; Zacchini, S.; Dimitratos, N.; Albonetti, S. Pt and Pt/Sn carbonyl clusters as precursors for the synthesis of supported metal catalysts for the base-free oxidation of HMF. *Appl. Catal., A* **2019**, *588*, 3006−3310.
(18) Hayashi, E.; Yamaguchi, Y.; Kamata, K.; Tsunoda, N.; Kumagai, Y.; Oba, F.; Hara, M. Effect of MnO_2 Crystal Structure on Aerobic Oxidation of 5-Hydroxymethylfurfural to 2,5-Furandicarboxylic Acid. *J. Am. Chem. Soc.* **2019**, *141*, 890−900.
(19) Jin, M.; Yu, L.; Chen, H.; Ma, X.; Cui, K.; Wen, Z.; Ma, Z.; Sang, Y.; Chen, M.; Li, Y. Base-free selective conversion of 5-hydroxymethylfurfural to 2,5-furandicarboxylic acid over a CoO_x-CeO_2 catalyst. *Catal. Today* **2021**, *367*, 2−8.
(20) Thao, N. T.; Kim Huyen, L. T. Enhanced catalytic performance of Cr-inserted hydrotalcites in the liquid oxidation of styrene. *J. Ind. Eng. Chem.* **2019**, *73*, 221−232.
(21) Zhou, W.; Liu, J.; Pan, J.; Sun, F. a.; He, M.; Chen, Q. Effect of Mg^{2+} on the catalytic activities of CoMgAl hydrotalcites in the selective oxidation of benzyl alcohol to benzaldehyde. *Catal. Commun.* **2015**, *69*, 1−4.
(22) Zhou, W.; Chen, G.; Yu, B.; Zhou, J.; Qian, J.; He, M.; Chen, Q. Efficient selective oxidation of benzyl alcohol with oxygen in a continuous fixed bed reactor over NiGa hydrotalcite derived catalyst. *Appl. Catal., A* **2020**, *592*, 117417−117426.
(23) Neaţu, F.; Petrea, N.; Petre, R.; Somoghi, V.; Florea, M.; Parvulescu, V. I. Oxidation of 5-hydroxymethyl furfural to 2,5-diformylfuran in aqueous media over heterogeneous manganese based catalysts. *Catal. Today* **2016**, *278*, 66−73.
(24) Raut, A. B.; Bhanage, B. M. Co-Al Hydrotalcites: Highly Active Catalysts for the One-Pot Conversion of Fructose to 2,5-Diformylfuran. *ChemistrySelect* **2018**, *3*, 11388−11397.
(25) Zhu, B.; Lin, B.; Zhou, Y.; Sun, P.; Yao, Q.; Chen, Y.; Gao, B. Enhanced photocatalytic H2 evolution on ZnS loaded with graphene and MoS_2 nanosheets as cocatalysts. *J. Mater. Chem. A* **2014**, *2*, 3819−3827.
(26) Berner, S.; Araya, P.; Govan, J.; Palza, H. Cu/Al and Cu/Cr based layered double hydroxide nanoparticles as adsorption materials for water treatment. *J. Ind. Eng. Chem.* **2018**, *59*, 134−140.
(27) Liu, C.; Li, C.; Chang, J. Effect of reaction time & calcination temperature on the properties of the NiAl-LDHs. *Spec. Petrochem.* **2017**, *34*, 17−22.
(28) Duan, Y.; Jia, F.; Wang, S.; Li, L. Synthesis and thermosensitivity of poly (N-isopropylacrylamide) / hydrotalcite hydrogel. *Chin. J. Appl. Chem.* **2018**, *35*, 102−108.
(29) Greenwell, H. C.; Holliman, P. J.; Jones, W.; Velasco, B. V. Studies of the effects of synthetic procedure on base catalysis using hydroxide-intercalated layer double hydroxides. *Catal. Today* **2006**, *114*, 397−402.
(30) Tien Thao, N.; Kim Huyen, L. T. Catalytic oxidation of styrene over Cu-doped hydrotalcites. *Chem. Eng. J.* **2015**, *279*, 840−850.
(31) Thao, N. T.; Trung, H. H. Selective oxidation of styrene over Mg−Co−Al hydrotalcite like-catalysts using air as oxidant. *Catal. Commun.* **2014**, *45*, 153−157.
(32) Mountapmbeme Kouotou, P.; Vieker, H.; Tian, Z. Y.; Tchoua Ngamou, P. H.; El Kasmi, A.; Beyer, A.; Gölzhäuser, A.; Kohse-Höinghaus, K. Structure−activity relation of spinel-type Co−Fe oxides for low-temperature CO oxidation. *Catal. Sci. Technol.* **2014**, *4*, 3359−3367.
(33) Nie, J.; Liu, H. Efficient aerobic oxidation of 5-hydroxymethylfurfural to 2,5-diformylfuran on manganese oxide catalysts. *J. Catal.* **2014**, *316*, 57−66.
(34) Huang, J.; Liu, B.; Fu, W. Preparation of Mg-Al hydrotalcite-supported Cr(VI), Mn(VII) and IO_4∼− catalysts and their performances for alcohols oxidation. *Nat. Gas Chem. Ind.* **2010**, *35*, 34−38.
(35) Huang, K.; Chu, X.; Yuan, L.; Feng, W.; Wu, X.; Wang, X.; Feng, S. Engineering the surface of perovskite $La_{0.5}Sr_{0.5}MnO_3$ for catalytic activity of CO oxidation. *Chem. Commum.* **2014**, *50*, 9200−9203.
(36) Choudhary, H.; Nishimura, S.; Ebitani, K. Metal-free oxidative synthesis of succinic acid from biomass-derived furan compounds using a solid acid catalyst with hydrogen peroxide. *Appl. Catal., A* **2013**, *458*, 55−62.
(37) Yu, L.; Chen, H.; Wen, Z.; Jin, M.; Ma, Z.; Ma, X.; Sang, Y.; Chen, M.; Li, Y. Highly selective oxidation of 5-hydroxymethylfurfural to 2,5-diformylfuran over an α-MnO_2 catalyst. *Catal. Today* **2021**, *367*, 9−15.
(38) Liao, L.; Liu, Y.; Li, Z.; Zhuang, J.; Zhou, Y.; Chen, S. Catalytic aerobic oxidation of 5-hydroxymethylfurfural into 2,5-diformylfuran over $VO^{2+}$and Cu^{2+}immobilized on amino-functionalized core−shell magnetic Fe3O4@SiO2. *RSC Adv.* **2016**, *6*, 94976−94988.
(39) Neaţu, F.; Marin, R. S.; Florea, M.; Petrea, N.; Pavel, O. D.; Pârvulescu, V. I. Selective oxidation of 5-hydroxymethyl furfural over non-precious metal heterogeneous catalysts. *Appl. Catal., B* **2016**, *180*, 751−757.
(40) Wan, X.; Zhou, C.; Chen, J.; Deng, W.; Zhang, Q.; Yang, Y.; Wang, Y. Base-Free Aerobic Oxidation of 5-Hydroxymethyl-furfural to 2,5-Furandicarboxylic Acid in Water Catalyzed by Functionalized Carbon Nanotube-Supported Au−Pd Alloy Nanoparticles. *ACS Catal.* **2014**, *4*, 2175−2185.

https://doi.org/10.1021/acs.iecr.2c00886
Ind. Eng. Chem. Res. 2022, 61, 11597−11603